AIAA JOURNAL
Vol. 51, No. 4, April 2013

Energy-Release Rate and Mode Mixity of Face/Core Debonds in Sandwich Beams

George A. Kardomateas*
Georgia Institute of Technology, Atlanta, Georgia 30332-0150
Christian Berggreen†
Technical University of Denmark, 2800 Lyngby, Denmark
and
Leif A. Carlsson‡
Florida Atlantic University, Boca Raton, Florida 33431

DOI: 10.2514/1.J051765

Closed-form algebraic expressions for the energy-release rate and the mode mixity are obtained for a debonded sandwich (trimaterial). The most general case of an "asymmetric" sandwich is considered (i.e., the bottom face sheet not necessarily of the same material or thickness as the top face sheet). The energy-release rate is obtained by use of the J-integral, and the expression is derived in terms of the forces and moments at the debond section. Regarding the mode mixity, a closed-form expression is derived in terms of the geometry, material, and applied loading, and it is proven that, in the trimaterial case, just as in the bimaterial case, the mode mixity can be obtained in terms of a single scalar quantity ω, which is independent of loading; the ω value for a particular geometry and material can be extracted from a numerical solution for one loading combination. Thus, this analysis extends the existing formulas in the literature, which are for either a delamination in a homogeneous composite or an interface crack in a bimaterial. These new "trimaterial with a crack" formulas are also proven to yield the formulas for the limits of a bimaterial or for a homogeneous section with a crack.

Nomenclature

D_d	=	bending rigidity of the debonded part
D_b	=	bending rigidity of the base part
D_s	=	bending rigidity of the substrate part
E_c	=	Young's modulus of the core, assumed to be equal in tension and compression
E_{f1}	=	Young's modulus of the top face sheet, assumed to be equal in tension and compression
E_{f2}	=	Young's modulus of the bottom face sheet, assumed to be equal in tension and compression
e_b	=	distance of neutral axis of base part from middle of core
e_s	=	distance of neutral axis of substrate from middle of core
G	=	energy-release rate
h_c	=	thickness of the core
h_{f1}	=	thickness of the top face sheet
h_{f2}	=	thickness of the bottom face sheet
J	=	J-integral
K	=	stress intensity factor
β	=	Dundur's bimaterial parameter
ϵ	=	bimaterial constant (oscillation index)
ψ	=	mode-mixity phase angle

Subscripts

d	=	debonded part
b	=	base part
s	=	substrate part

Superscripts

d	=	debonded part
b	=	base part
s	=	substrate part

I. Introduction

TYPICAL sandwich panels consist of two stiff metallic or composite thin face sheets separated by a soft/stiff honeycomb or foam thick core of low/high density. This configuration gives the sandwich material system high stiffness and strength with little resultant weight penalty and high-energy-absorption capability related to the application of sandwich structures in the construction of aerospace vehicles (especially rotorcraft), naval vehicles, and wind turbines.

In these sandwich structures, the interface between the face sheet and the core is justifiably considered to be the weak link. This is because debonding may occur at this interface, and such debonds could grow and eventually completely delaminate the face sheet. The most common cause of these defects is poor or missing bonding due to careless manufacturing or a mismatch in the geometry. Similar defects may also arise during service due to thermomechanical loads, impact events, or structural fatigue. The latter decohesion is induced primarily due to the elastic and/or thermal mismatch between face sheet and core.

A loading that can be especially detrimental is compression because these debonds are susceptible to buckling and subsequent rapid growth during the postbuckling phase. Typically, postbuckling solutions are derived in terms of forces and moments at the debond section for both sandwich [1] or monolithic composites [2,3]. Therefore, expressions for the energy-release rate in terms of these quantities are particularly useful. Such an expression was first derived by Yin and Wang [4] for a delaminated homogeneous composite; it was subsequently extended by Suo and Hutchinson [5] to a delaminated bimaterial (thin film on a substrate). The sandwich configuration is, however, a "trimaterial" (i.e., two face sheets), which need not be the same, and a core in the middle. This is the configuration treated in this paper. Specifically, we use the J-integral

Received 11 December 2011; revision received 10 June 2012; accepted for publication 23 June 2012; published online 7 February 2013.

*Professor, School of Aerospace Engineering.
†Associate Professor, Department of Mechanical Engineering.
‡Professor, Department of Mechanical Engineering.

to obtain a closed-form algebraic expression for the energy-release rate G of a debonded sandwich plate. The most general case of an asymmetric sandwich is considered (i.e., the bottom face sheet not necessarily of the same material or thickness as the top face sheet). The expression derived is in terms of the debond forces and moments, which are typical outputs of postbuckling solutions. It should be noted that the case of an interface crack in a symmetric sandwich was also treated in Ostergaard and Sorensen [6], but that work contains a derivation error.

In this paper, following the derivation of the energy-release rate for a debond in a general asymmetric sandwich beam (a trimaterial), the mode mixity is derived by following the approach of Suo and Hutchinson [5] for a bimaterial. The approach is based on the assumption of a constant scalar quantity ω, which enters in the complex stress intensity factor expressions. This quantity is assumed to depend only on the geometry and material and not the loading. Under the same assumption of a constant ω, we derive the relevant relationships for the mode mixity of a trimaterial. This assumption is then critically tested by extensive finite-element analyses (FEAs) for a soft-core and a moderate-core sandwich configuration and six different loading combinations. It is clearly shown that this ω is nearly constant in all cases. It is also proven that the present formulas yield the results in the literature for the bimaterial or the homogeneous material limiting cases.

II. Analysis for the Energy-Release Rate

We consider a sandwich beam consisting of face sheets of thicknesses h_{f1} and h_{f2} and Young's moduli E_{f1} and E_{f2}, respectively (assumed to be equal in tension and compression), and a core of thickness h_c, with a Young's modulus E_c, again assumed to be equal in tension and compression (Fig. 1a). Over the region of the debond, the sandwich beam consists of two parts: the debonded upper face sheet (referred to as the "debonded part", of thickness h_{f1}) and the part below the debond ("substrate part," of thickness $h_c + h_{f2}$, which includes the core and the lower face sheet). A unit width is assumed. The intact region of the beam to the right of the debond is referred to as the "base part" and consists of the entire section of the sandwich beam of thickness $h_{f1} + h_c + h_{f2}$. We shall denote the base part as "b", the debonded part as "d", and the substrate part as "s".

A characteristic of a sandwich beam with a debond is that the neutral axes for the base and the substrate parts are, in general, no longer at the geometrical midpoints of the corresponding sections. With respect to a reference axis x through the middle of the core, the neutral axis of the base section is located at a distance e_b (Fig. 1a), given by

$$e_b(E_{f1}h_{f1} + E_c h_c + E_{f2}h_{f2}) = E_{f2}h_{f2}\left(\frac{h_{f2}}{2} + \frac{h_c}{2}\right) - E_{f1}h_{f1}\left(\frac{h_{f1}}{2} + \frac{h_c}{2}\right) \tag{1a}$$

The neutral axis of the substrate part is at a distance e_s:

$$e_s[E_c h_c + E_{f2}h_{f2}] = E_{f2}h_{f2}\left(\frac{h_{f2}}{2} + \frac{h_c}{2}\right) \tag{1b}$$

Moreover, for the debonded face sheet, which is homogeneous, the bending rigidity per unit width is

$$D_d = E_{f1}\frac{h_{f1}^3}{12} \tag{2a}$$

And for the base part the flexural rigidity per unit width, it is (Fig. 1a)

$$D_b = E_{f1}\frac{h_{f1}^3}{12} + E_{f1}h_{f1}\left(\frac{h_{f1}}{2} + \frac{h_c}{2} + e_b\right)^2 + E_{f2}\frac{h_{f2}^3}{12} + E_{f2}h_{f2}\left(\frac{h_{f2}}{2} + \frac{h_c}{2} - e_b\right)^2 + E_c\frac{h_c^3}{12} + E_c h_c e_b^2 \tag{2b}$$

and for the substrate (again, per unit width), it is

$$D_s = E_c\frac{h_c^3}{12} + E_c h_c e_s^2 + E_{f2}\frac{h_{f2}^3}{12} + E_{f2}h_{f2}\left(\frac{h_{f2}}{2} + \frac{h_c}{2} - e_s\right)^2 \tag{2c}$$

Figure 1a shows a segment of the beam containing the debond front (crack tip).

A section of the beam ahead of the crack tip carries the compressive axial force P_b and bending moment M_b, both per unit width (base part loads).

Behind the crack tip, the cross section above the debond (debonded part) carries the loads P_d and M_d, and the cross section below the debond (substrate part) carries the loads P_s and M_s. It is assumed that these forces and moments have already been determined from the postbuckling solution of the plate. It should be noted that, in this derivation, we consider only the effects of the axial forces and bending moments; transverse shear forces are neglected.

Equilibrium of forces and moments (about the neutral axis of the base part) yields

$$P_b = P_d + P_s \tag{3a}$$

$$M_b - M_d - M_s - P_d\left(\frac{h_{f1}}{2} + \frac{h_c}{2} + e_b\right) + P_s(e_s - e_b) = 0 \tag{3b}$$

If we set

$$(EA)_b = E_{f1}h_{f1} + E_c h_c + E_{f2}h_{f2} \tag{4}$$

then the axial stresses in the upper and lower face sheets and the core in the base part are

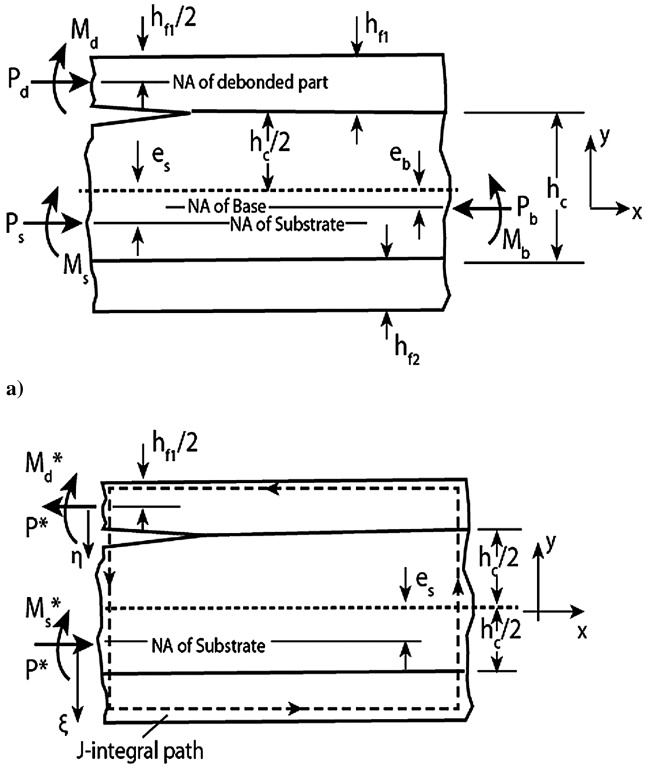

Fig. 1 a) Sandwich elements with the acting forces and moments, and b) The J-integral path.

$$\sigma_{xx}^{(b)} = \begin{cases} -\frac{P_b}{(EA)_b}E_{f1} - \frac{M_b E_{f1}}{D_b}y & \text{if } e_b + \frac{h_c}{2} \le y \le e_b + \frac{h_c}{2} + h_{f1} \text{ [debonded face]} \\ -\frac{P_b}{(EA)_b}E_c - \frac{M_b E_c}{D_b}y & \text{if } e_b - \frac{h_c}{2} \le y \le e_b + \frac{h_c}{2} \text{ [core]} \\ -\frac{P_b}{(EA)_b}E_{f2} - \frac{M_b E_{f2}}{D_b}y & \text{if } e_b - \frac{h_c}{2} - h_{f2} \le y \le e_b - \frac{h_c}{2} \text{ [lower face]} \end{cases} \tag{5}$$

Following the approach by Suo and Hutchinson [5] for a bimaterial problem, superimposing $-\sigma_{xx}^{(b)}$ on the stresses behind and ahead of the debond front in the system in Fig. 1a, would result in the system in Fig. 1b, whose energy-release rate and stress intensity factors would be the same as in the original system (Fig. 1a) because the system of base part stresses acting alone would produce a nonsingular stress field. In this way, we can have two parameters, P^* and M_d^*, in terms of which the energy-release rate may be expressed.

Therefore, the forces acting in the system in Fig. 1b are

$$P^* = \int_{e_b+\frac{h_c}{2}}^{e_b+\frac{h_c}{2}+h_{f1}} (-\sigma_{xx}^{(b)})\,\mathrm{d}y - P_d \tag{6}$$

Substituting $\sigma_{xx}^{(b)}$ from Eq. (5) and performing the integration results in P^* in the following form:

$$P^* = C_1 P_b + C_2 M_b - P_d \tag{7a}$$

where

$$C_1 = \frac{E_{f1}h_{f1}}{(EA)_b}; \qquad C_2 = \frac{E_{f1}h_{f1}}{2D_b}(2e_b + h_{f1} + h_c) \tag{7b}$$

Likewise,

$$M_d^* = M_d - \int_{e_b+\frac{h_c}{2}}^{e_b+\frac{h_c}{2}+h_{f1}} (-\sigma_{xx}^{(b)})\left[y - \left(e_b + \frac{h_c}{2} + \frac{h_{f1}}{2}\right)\right]\mathrm{d}y \tag{8}$$

Substituting again $\sigma_{xx}^{(b)}$ from Eq. (5) and performing the integration results in M_d^* in the following form:

$$M_d^* = M_d - C_3 M_b \tag{9a}$$

where

$$C_3 = \frac{E_{f1}}{D_b}\frac{h_{f1}^3}{12} \tag{9b}$$

The corresponding moment M_s^* in the substrate part, is obtained from equilibrium (Fig. 1b):

$$M_s^* = P^*\left(e_s + \frac{h_c}{2} + \frac{h_{f1}}{2}\right) - M_d^* \tag{10}$$

Referring now to Fig. 1b, the stresses acting on the debonded face produced by the tensile load P^* and the bending moment M_d^* are

$$\sigma_{xx} = \frac{P^*}{h_{f1}} + E_{f1}\frac{M_d^*}{D_d}\eta; \qquad -\frac{h_{f1}}{2} \le \eta \le \frac{h_{f1}}{2} \tag{11a}$$

$$\sigma_{yy} = \tau_{xy} \simeq 0 \tag{11b}$$

where η is a vertical coordinate measured from the midplane of the debonded face.

In Fig. 1b, the cross section of the sandwich ahead of the debond front is subject to vanishing stress and strain. In the region behind the debond front, we have $\epsilon_{zz} = 0$ (plane strain). It follows that

$$\sigma_{zz} = \nu_{xz}^{(f1)}\sigma_{xx}; \qquad \epsilon_{xx} = \frac{\sigma_{xx} - \nu_{zx}^{(f1)}\sigma_{zz}}{E_{f1}} = \frac{1 - \nu_{zx}^{(f1)}\nu_{xz}^{(f1)}}{E_{f1}}\sigma_{xx} \tag{12}$$

where $\nu_{xz}^{(f1)}$ and $\nu_{zx}^{(f1)}$ are the Poisson ratios of the debonded (orthotropic) face sheet.

Considering now the J-integral path shown in Fig. 1b, the following expression holds along the vertical path across the debonded face:

$$\mathrm{d}J = W\mathrm{d}y - \mathbf{T}\frac{\partial \mathbf{u}}{\partial x}\mathrm{d}s; \qquad \mathrm{d}y = -\mathrm{d}s \tag{13}$$

where W is the strain energy density, $\mathbf{T}$ is the traction vector, and $\mathbf{u}$ is the displacement vector [7].

Because

$$W = \frac{1}{2}(\sigma_{xx}\epsilon_{xx} + \sigma_{zz}\epsilon_{zz}) = \frac{1}{2}\sigma_{xx}\epsilon_{xx}; \qquad \mathbf{T}\frac{\partial \mathbf{u}}{\partial x} = -\sigma_{xx}\epsilon_{xx} \tag{14a}$$

and because $\mathrm{d}s = \mathrm{d}\eta$, and by use of Eq. (12),

$$\mathrm{d}J = -\frac{1}{2}\sigma_{xx}\epsilon_{xx}\mathrm{d}s + \sigma_{xx}\epsilon_{xx}\mathrm{d}s = \frac{1}{2}\sigma_{xx}\epsilon_{xx}\mathrm{d}s = \frac{1 - \nu_{zx}^{(f1)}\nu_{xz}^{(f1)}}{E_{f1}}\sigma_{xx}^2\mathrm{d}\eta \tag{14b}$$

Substituting σ_{xx} from Eq. (11a), we obtain the contribution from the debonded face to the J-integral:

$$\begin{aligned} J_1 &= \int_{-\frac{h_{f1}}{2}}^{\frac{h_{f1}}{2}} \frac{(1 - \nu_{zx}^{(f1)}\nu_{xz}^{(f1)})}{2E_{f1}}\left(\frac{P^*}{h_{f1}} + E_{f1}\frac{M_d^*}{D_d}\eta\right)^2 \mathrm{d}\eta \\ &= \frac{(1 - \nu_{zx}^{(f1)}\nu_{xz}^{(f1)})}{2E_{f1}}\left(\frac{P^{*2}}{h_{f1}} + E_{f1}^2\frac{M_d^{*2}}{D_d^2}\frac{h_{f1}^3}{12}\right) \end{aligned} \tag{15}$$

Similarly, if we set

$$(EA)_s = E_c h_c + E_{f2}h_{f2} \tag{16}$$

then the stresses in the cross section below the debond in Fig. 1b, which are produced by the compressive force P^* and the bending moment M_s^*, are:

$$\sigma_{xx} = \begin{cases} -\frac{P^*}{(EA)_s}E_c + \frac{M_s^* E_c}{D_s}\xi & \text{if } -e_s - \frac{h_c}{2} \le \xi \le -e_s + \frac{h_c}{2} \text{ [core]} \\ -\frac{P^*}{(EA)_s}E_{f2} + \frac{M_s^* E_{f2}}{D_s}\xi & \text{if } -e_s + \frac{h_c}{2} \le \xi \le -e_s + \frac{h_c}{2} + h_{f2} \text{ [lower face]} \end{cases} \tag{17a}$$

and

$$\sigma_{yy} = \tau_{xy} \simeq 0 \tag{17b}$$

where ξ is a normal coordinate measured from the neutral axis of this cross section. Again, following the same arguments as before, i.e., that the cross section of the sandwich ahead of the debond front is subjected to vanishing stress and strain and that in the region behind the debond front we have $\epsilon_{zz} = 0$ (plane strain), we obtain the the following expression for the J integral contribution from the vertical path below the debond:

$$\mathrm{d}J = \frac{1}{2}\sigma_{xx}\epsilon_{xx}\mathrm{d}s - \sigma_{xx}\epsilon_{xx}\mathrm{d}s = \frac{1 - \nu_{zx}^{(i)}\nu_{xz}^{(i)}}{E_i}\sigma_{xx}^{(i)2}\mathrm{d}\xi \tag{18a}$$

where i refers to the core (c) or the lower face sheet ($f2$).

Hence, the total contribution from the vertical path below the debond to the J-integral is:

$$J_2 = \int_{-e_s-\frac{h_c}{2}}^{-e_s+\frac{h_c}{2}} \frac{(1-\nu_{zx}^{(c)}\nu_{xz}^{(c)})}{2E_c}\sigma_{xx}^{(c)2}\,\mathrm{d}\xi + \int_{-e_s+\frac{h_c}{2}}^{-e_s+\frac{h_c}{2}+h_{f2}} \frac{(1-\nu_{zx}^{(f2)}\nu_{xz}^{(f2)})}{2E_{f2}}\sigma_{xx}^{(f2)2}\,\mathrm{d}\xi \tag{18b}$$

Substituting the corresponding expressions for the core and lower face stresses from Eq. (17a) and performing the integration leads to

$$J_2 = \frac{P^{*2}}{(EA)_s^2}H_1 + \frac{P^*M_s^*}{(EA)_sD_s}H_2 + \frac{M_s^{*2}}{D_s^2}H_3 \tag{19a}$$

where

$$H_1 = \frac{1-\nu_{zx}^{(c)}\nu_{xz}^{(c)}}{2}E_ch_c + \frac{1-\nu_{zx}^{(f2)}\nu_{xz}^{(f2)}}{2}E_{f2}h_{f2} \tag{19b}$$

$$H_2 = \frac{1-\nu_{zx}^{(c)}\nu_{xz}^{(c)}}{2}E_ch_c2e_s + \frac{1-\nu_{zx}^{(f2)}\nu_{xz}^{(f2)}}{2}E_{f2}h_{f2}(2e_s-h_c-h_{f2}) \tag{19c}$$

and

$$H_3 = \frac{1-\nu_{zx}^{(c)}\nu_{xz}^{(c)}}{2}E_ch_c\left(\frac{h_c^2}{12}+e_s^2\right) + \frac{1-\nu_{zx}^{(f2)}\nu_{xz}^{(f2)}}{2}E_{f2}h_{f2}\left[\frac{h_{f2}^2}{3}+\left(\frac{h_c}{2}-e_s\right)\left(\frac{h_c}{2}+h_{f2}-e_s\right)\right] \tag{19d}$$

The sum of the two integrals of Eqs. (15, 19a) delivers the energy-release rate because the remaining portions of the path make no contribution to the J-integral, i.e.,

$$G = J_1 + J_2 \tag{20}$$

or

$$G = \frac{(1-\nu_{zx}^{(f1)}\nu_{xz}^{(f1)})}{2E_{f1}}\left(\frac{P^{*2}}{h_{f1}}+E_{f1}^2\frac{M_d^{*2}}{D_d^2}\frac{h_{f1}^3}{12}\right) + \left(\frac{P^{*2}}{(EA)_s^2}H_1 + \frac{P^*M_s^*}{(EA)_sD_s}H_2 + \frac{M_s^{*2}}{D_s^2}H_3\right) \tag{21}$$

where H_1, H_2, and H_3 are given in Eqs. (19b–19d).

III. Stress Intensity Factor Expressions for the Asymmetric TriMaterial

Substituting Eq. (10) for M_s^* into Eq. (21), we can write the energy-release rate in the following form:

$$G = a_1P^{*2} + a_2M_d^{*2} - a_3P^*M_d^* \tag{22}$$

where

$$a_1 = \frac{(1-\nu_{zx}^{(f1)}\nu_{xz}^{(f1)})}{2E_{f1}h_{f1}} + \frac{H_1}{(EA)_s^2} + \frac{H_2}{(EA)_sD_s}\left(e_s+\frac{h_c}{2}+\frac{h_{f1}}{2}\right) + \frac{H_3}{D_s^2}\left(e_s+\frac{h_c}{2}+\frac{h_{f1}}{2}\right)^2 \tag{23a}$$

$$a_2 = (1-\nu_{zx}^{(f1)}\nu_{xz}^{(f1)})\frac{E_{f1}h_{f1}^3}{24D_d^2} + \frac{H_3}{D_s^2} \tag{23b}$$

$$a_3 = \frac{H_2}{(EA)_sD_s} + 2\frac{H_3}{D_s^2}\left(e_s+\frac{h_c}{2}+\frac{h_{f1}}{2}\right) \tag{23c}$$

The face sheet/core debond is an interface crack between two distinct materials: the top face sheet ($f1$) and the core (c). Thus, we assume that the asymptotic field is governed by the bimaterial interface crack solution. The complex stress intensity factor $K = K_1 + iK_2$ has been introduced (Rice [8] and Hutchinson et al. [9]) such that the stress a distance r ahead of the crack tip is given by

$$\sigma_{yy} + i\tau_{xy} = \frac{K}{\sqrt{2\pi r}}r^{i\epsilon} \tag{24a}$$

where ϵ is the bimaterial constant (oscillation index):

$$\epsilon = \frac{1}{2\pi}\ln\frac{1-\beta}{1+\beta} \tag{24b}$$

In the previous expression, β is the Dundur's bimaterial parameter:

$$\beta = \frac{G_{f1}(\kappa_c-1) - G_c(\kappa_{f1}-1)}{G_{f1}(\kappa_c+1) + G_c(\kappa_{f1}+1)} \tag{24c}$$

where

$$\kappa = \begin{cases} 3-4\nu & \text{for plane strain} \\ (3-\nu)/(1+\nu) & \text{for plane stress} \end{cases} \tag{24d}$$

In the previous expressions, G_k is the shear modulus, and ν_k is the Poisson's ratio for the upper face sheet, $k = f1$, and for the core, $k = c$.

In addition, the energy-release rate in terms of the complex stress intensity factor K is

$$G = B|K|^2 \tag{25a}$$

where

$$B = \frac{G_c(\kappa_{f1}+1) + G_{f1}(\kappa_c+1)}{16G_{f1}G_c\cosh^2\pi\varepsilon} \tag{25b}$$

Therefore, by using Eq. (22), we obtain

$$|K|^2 = \frac{1}{B}(a_1P^{*2} + a_2M_d^{*2} - a_3P^*M_d^*) \tag{26}$$

To determine the real and imaginary parts of the complex stress intensity factor, arguments similar to Thouless et al. [10] and Hutchinson et al. [9] are exploited, as was also done in Suo and Hutchinson [5], based on dimensional considerations and linearity. Thus, we can write the complex stress intensity factor K in the following form:

$$K = \frac{1}{\sqrt{B}}\left(-aP^*\sqrt{a_1} + bM_d^*\sqrt{a_2}\right)h_{f1}^{-i\epsilon} \tag{27}$$

where a and b are complex numbers that depend on the geometry and material properties but not on the loading.

From Eq. (26), we obtain in a similar fashion as in Suo and Hutchinson [5]:

$$a = e^{i\omega}, \qquad b = -ie^{i(\omega+\gamma)} \tag{28}$$

Notice that, because in this process we are essentially taking the square root of Eq. (26), there is a second solution that can be obtained; this can be achieved by setting a positive sign in front of the b expression in Eq. (28). The first solution, outlined hereby, leads to a value of ω that is practically independent of loading (as will be proven later); however, the second solution would lead to a ω being strongly

dependent on loading, which would invalidate the assumption of a and b being complex numbers independent of loading and would be of no use in establishing a closed-form approach for the mode mixity. The fact that the second solution would not lead to a constant ω was firmly established from our extensive numerical results.

Now, we can rewrite Eq. (27) as

$$K = K_1 + iK_2 = \frac{1}{\sqrt{B}}\left(-P^*\sqrt{a_1} - ie^{i\gamma}M_d^*\sqrt{a_2}\right)h_{f1}^{-i\epsilon}e^{i\omega} \tag{29a}$$

where

$$\sin\gamma = \frac{a_3}{2\sqrt{a_1 a_2}} \tag{29b}$$

Thus, we only need determine the parameter ω, which should depend only on the materials and geometry (but not on the loading).

For the determination of the mode-mixity phase angle, we shall follow the suggestion in Rice [8], Hutchinson et al. [9], and Charalambides et al. [11] to consider $Kh_{f1}^{i\epsilon}$ because $|K| = |Kh_{f1}^{i\epsilon}|$. In this way, we obtain

$$Re[Kh_{f1}^{i\epsilon}] = \frac{1}{\sqrt{B}}\left[-P^*\sqrt{a_1}\cos\omega + M_d^*\sqrt{a_2}\sin(\omega+\gamma)\right] \tag{30a}$$

$$\mathrm{Im}[Kh_{f1}^{i\epsilon}] = \frac{1}{\sqrt{B}}\left[-P^*\sqrt{a_1}\sin\omega - M_d^*\sqrt{a_2}\cos(\omega+\gamma)\right] \tag{30b}$$

We can thus define the phase angle or mode mixity ψ, from

$$Kh_{f1}^{i\epsilon} = |K|e^{i\psi} \tag{31}$$

Because $Re[Kh_{f1}^{i\epsilon}] = |K|\cos\psi$ and $\mathrm{Im}[Kh_{f1}^{i\epsilon}] = |K|\sin\psi$, we obtain an expression for ψ by using Eqs. (30a, 30b) as

$$\tan\psi = \frac{\lambda\sin\omega - \cos(\omega+\gamma)}{\lambda\cos\omega + \sin(\omega+\gamma)} \tag{31a}$$

where

$$\lambda = -\frac{P^*}{M_d^*}\sqrt{\frac{a_1}{a_2}} \tag{31b}$$

The structure of Eq. (31a) is similar to the one in Suo and Hutchinson [5], which is for a bimaterial, but the λ expression in Eq. (31b) is for a "trimaterial", i.e., it includes the effect of the lower face sheet through the a_1 and a_2 expressions defined in Eqs. (23a, 23b) and the γ expression defined in Eqs. (29b, 23c). Note also that the force P^* defined in this paper is of sign opposite to the corresponding load in [3].

Finite-element analysis will allow calculating the angle ω from Eq. (31a) as follows:

$$\omega = \tan^{-1}\left[\frac{\cos\gamma + (\lambda+\sin\gamma)\tan\psi}{\lambda + \sin\gamma - \cos\gamma\tan\psi}\right] \tag{31c}$$

and examining if this is constant for a sandwich with fixed material and geometric configuration under different loadings. This is the subject of the next section.

IV. Extraction of ω from Finite-Element Analysis

The double cantilever beam specimen with uneven bending moments (DCB-UBM), introduced by Sorensen et al. [12] and later modified for sandwich specimens by Lundsgaard-Larsen et al. [13], also described in the book by Carlsson and Kardomateas [14] (see Fig. 2), was chosen for extraction of the ω parameter in Eq. (31a) from finite-element analysis. The DCB-UBM specimen was chosen due to the pure bending state in the specimen compatible with the analysis

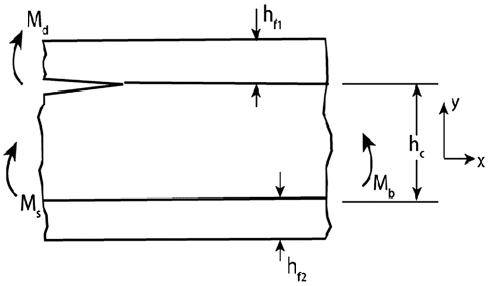

Fig. 2 Moment loading of DCB-UBM specimen.

presented previously. Furthermore, to investigate the variation of the ω parameter for a range of mode-mixity phase angles, the DCB-UBM specimen allows for easy variation of the mode-mixity phase angle (ψ) at the crack tip through changing the ratio between the two edge moments; see Fig. 2.

Three demonstration cases were chosen to demonstrate the procedure to determine the ω parameter for a specific material system as well as to demonstrate the applicability of the analytical model for typical material combinations. The three test-case specimens are illustrated in Fig. 3. Specifically, two sandwich cases (Fig. 3a) with moderate and high stiffness mismatch over the face/core interface and a bimaterial case (Fig. 3b) with a moderate stiffness mismatch were examined. The geometry of the sandwich specimens were chosen to reflect typical face/core thickness ratios. The face thickness was constant for all cases, $h_f = 2$ mm. For the bimaterial case, the thickness of the thinner layer was kept equal to the face sheet thicknesses in the sandwich cases, whereas the thicker layer was chosen as the thickness of the core plus a face sheet from the sandwich cases. The core thicknesses for the sandwich and bimaterial cases were 20 and 22 mm, respectively. Furthermore, the length of the specimens were chosen sufficiently long ($L = 500$ mm) so that shear stress fields originating from the crack tip region did not reach the specimen edges and thus did not violate the assumptions in the analytical model.

The crack length was $a = 200$ mm for all cases. We have examined two symmetric sandwich configurations and in both cases the face remains the same (i.e., aluminum). One of the cases involves a soft core (H100) and the other a moderate core (aluminum foam). We have also examined a bimaterial case consisting of one layer of aluminum and one of aluminum foam. The material properties are summarized in Table 1.

A. Details of the Finite-Element Model

Two-dimensional models of the sandwich and bimaterial DCB-UBM specimens were developed using the ANSYS commercial finite-element code. The face sheet, core, and bimaterials were

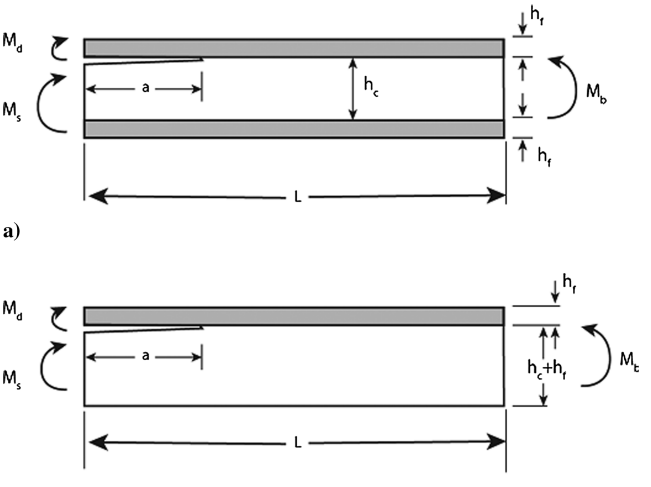

Fig. 3 a) Loading of sandwich element, and b) bimaterial element.

Table 1 Material properties and geometry

Aluminum face (isotropic)	H100 core (orthotropic)	Aluminum foam core (orthotropic)
$E = 70,000$ MPa	$E_x = E_y = E_z = 130$ MPa	$E_x = E_y = E_z = 7,000$ MPa
$G = 26,923$ MPa	$G_{xy} = G_{yz} = G_{zx} = 35$ MPa	$G_{xy} = G_{yz} = G_{zx} = 2,692.3$ MPa
$\nu = 0.30$	$\nu_{xy} = \nu_{yz} = \nu_{zx} = 0.32$	$\nu_{xy} = \nu_{yz} = \nu_{zx} = 0.32$

assumed to be isotropic and linear elastic (Table 1). Isoparametric two-dimensional four- and eight-node elements (PLANE42 and PLANE82) were used in the models, where the crack-tip region was modeled using a highly refined mesh (Fig. 4), allowing an accurate fracture analysis. The cracked region of the specimen was meshed using a double set of nodes along the cracked interface. No contact elements were used at the cracked interface.

To properly apply loads and boundary conditions on the model, mimicking the bending moments and the reaction moment in the analytical model, multipurpose constraint (MPC) conditions were applied at the beam ends, enforcing the nodes at the end of the cracked beam to remain on a straight line. The bending moments M_d and M_s were then applied to two master nodes at the center left end of each beam. At the uncracked end of the specimen, clamping is simulated by restricting x and y displacements of the nodes on the upper and lower faces over a specific distance L_s ($L_s = 50$ mm) from the uncracked specimen end; see Fig. 4.

Finite-element simulations were used to calculate the mode-mixity phase angle ψ, defined in Eq. (31a).

The mode-mixity phase angle may be determined from the crack flank displacements (Berggreen et al. [15]):

$$\psi = \tan^{-1}\left(\frac{\delta_x}{\delta_y}\right) - \varepsilon \ln\left(\frac{x}{h}\right) + \tan^{-1}(2\varepsilon) \tag{32}$$

where δ_x and δ_y are the relative crack flank opening and shearing displacements, respectively, measured at a distance x behind the crack tip; ϵ is the oscillatory index defined in Eq. (24b); and h is the characteristic length, which for this case is chosen as the face-sheet thickness (or the smallest bimaterial thickness in case the bimaterial case). Both the mode-mixity phase angle ψ and the energy-release rate G were determined from the finite-element analysis using the CSDE (from "crack surface displacement extrapolation") method [15]. This method calculates the phase angle from the relative opening and shearing displacements along the crack flanks and extrapolates the values of phase angle and energy-release rate to the crack tip. This approach has been used in Berggreen et al. [15] and a more-detailed description can be found in that paper.

Three specimen configurations were analyzed according to the previous description, i.e., two sandwich cases (soft and moderate stiff cores) and one bimaterial with moderate stiff core. To vary the mode mixity, a large range of moment ratios M_d/M_s was examined. In all finite-element simulations, the magnitudes of M_d and M_s, Fig. 3, were selected to achieve an energy-release rate $G \simeq 400$ J/m^2. Subsequently, the ω were determined from Eq. (31c) where the ψ calculated from the finite-element analysis were used.

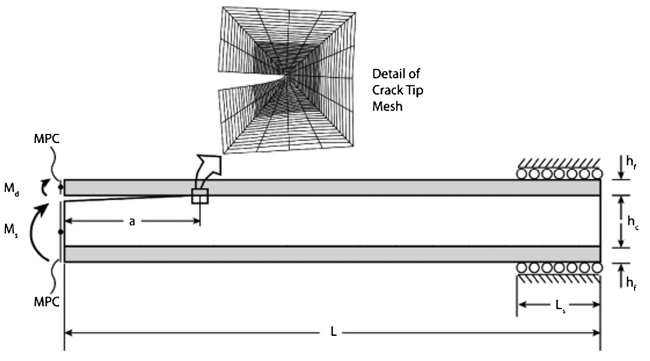

Fig. 4 Finite-element model of DCB-UBM specimen.

Table 2 H100 core (130 MPa) sandwich

M_d, N · mm	75.6	129.6	196.1	118.6	71.1
M_s, N · mm	−604.8	−518.4	−196.1	474.4	568.8
G_{anal} [Eq. (22)], N/mm	0.4239	0.4350	0.4140	0.3613	0.3727
G_{FEA}, N/mm	0.4076	0.4214	0.4107	0.3553	0.3626
ψ_{FEA}, deg	52.6	35.6	1.11	−68.5	−85.4
ω [Eq. (31c) with ψ_{FEA}], deg	74.09	73.66	73.34	73.74	73.54

Table 3 Aluminum foam core (7 GPa) sandwich

M_d, N · mm	8.340	76.80	157.7	199.4	159.5
M_s, Nmm	−4170.0	−3840.0	−2523.4	−199.4	2552.0
G_{anal} [Eq. (22)], N/mm	0.3969	0.3997	0.3963	0.3890	0.3862
G_{FEA}, N/mm	0.3848	0.3883	0.3895	0.3872	0.3819
ψ_{FEA}, deg	54.4	33.9	4.04	−30.9	−72.2
ω [Eq. (31c) with ψ_{FEA}], deg	58.20	57.60	56.87	56.34	56.04

Table 4 Bimaterial: aluminum (70 GPa) and aluminum foam (7 GPa)

M_d, N · mm	5.86	55.9	133.3	199.0	136.8
M_s, N · mm	−2930.0	−2795.0	−2132.8	−199.0	2188.8
G_{anal} [Eq. (22)], N/mm	0.3979	0.3997	0.3983	0.3890	0.3871
G_{FEA}, N/mm	0.3855	0.3875	0.3894	0.3871	0.3810
ψ_{FEA}, deg	54.9	40.1	14.0	−30.0	−84.1
ω [Eq. (31c) with ψ_{FEA}], deg	58.89	58.50	57.63	56.10	54.82

B. Results for ω Confirmation of the Nearly Constant ω Hypothesis

The first case considered was the sandwich with soft (130 MPa) core. The rsults listed in Table 2 show that the analytical expression [Eq. (22)] and the FEA provide energy-release rates that are in close agreement. The mode-mixity phase angle varies from 52.6 to −85.6 deg, and the parameter ω remains virtually constant with an average of 73.7 deg, and all values are within 0.6% of this value.

Results for the sandwich with a moderately stiff core are listed in Table 3. Again, the analytical solution and the FEA are in close agreement for the energy-release rate, and the parameter ω is almost constant, 57 deg on average, and all values are within 2.1% of this value. An interesting observation is that ω for the moderate core sandwich (Table 3) is less than ω for the soft core sandwich (Table 2). Another interesting observation is that the soft core gives the least variation in ω (most constant ω).

Table 4 (for a bimaterial, moderate core) gives an average ω of 57.19 deg, and all values are within 4.1% of this value. The values of ω from our analysis for the bimaterial limit (Table 4) are also confirmed by the corresponding values from the analysis of Suo and Hutchinson [5]. An interesting observation is that the trimaterial analysis results in more constant ω versus the corresponding bimaterial case.

Notice also that ω is very similar for the trimaterial beam with a moderately stiff core ($E_c = 7$ GPa) (Table 3) and the corresponding bimaterial configuration (Table 4). Further studies, however, must be conducted on other configurations, such as asymmetric sandwich beams.

Based on these results, the mode-mixity phase angle for any trimaterial, ψ, can be obtained from Eq. (31a) for any loading combination, after first extracting the ω value for the particular geometry and material from a numerical solution for just one loading combination.

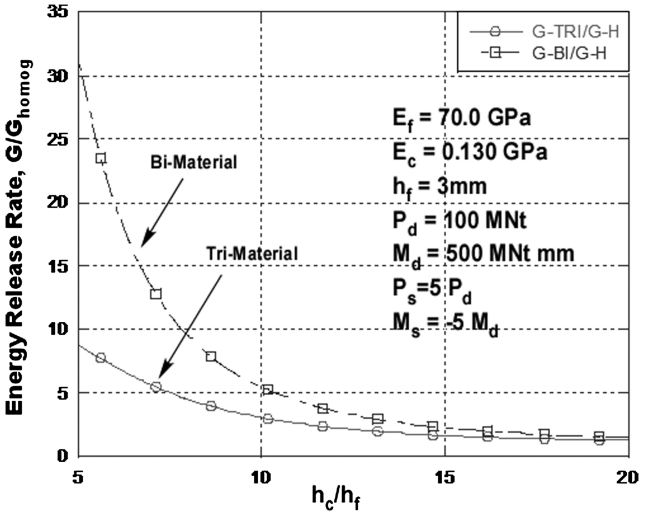

Fig. 5 Effect of core thickness on the energy-release rate.

V. Results on Energy-Release-Rate Trends

Let us first consider a sandwich configuration consisting of faces with $E_f = 70$ GPa and a core with $E_c = 130$ MPa, which are typical of aluminum faces and PVC foam core materials. The geometry is symmetric with $h_{f1} = h_{f2} = h_f = 3$ mm. The core thickness h_c is variable. The total thickness is $2h_f + h_c$. We shall first examine the effect of core thickness and, in particular, the ratio h_c/h_f on the energy-release rate. We assume a loading of $P_d = 100$ MN, $M_d = 500$ MN mm, $P_s = 5P_d$, and $M_s = -5M_d$.

We shall also examine a bimaterial beam consisting of a top layer of thickness h_f and face material (70 Gpa) and bottom layer of thickness $h_c + h_f$ and core material (130 MPa), i.e., the total thickness is still the same as the trimaterial case.

In the following results, we normalize with the energy-release rate for the corresponding homogeneous construction, i.e., if the entire section was made of the face sheet material (70 GPa).

Figure 5 shows the energy-release rate G plotted versus the core-to-face thickness ratio, obtained from both the trimaterial formula [Eq. (21)] and the bimaterial formula [5]. Because G is normalized with the corresponding homogeneous limit, the first observation that can be made is that a homogeneous section of face sheet material would have a lower energy-release rate than either the tri- or the bimaterial, actually substantially less for low ratios of h_c/h_f. The second observation to be made is that the bimaterial formula would result in a higher energy-release rate than the trimaterial formula, again substantially higher for the lower ratios of h_c/h_f. Actually, for $h_c/h_f = 10$, the energy-release rate from the trimaterial formula is about 43% less than the corresponding one from the bimaterial formula and three times that of the homogeneous formula.

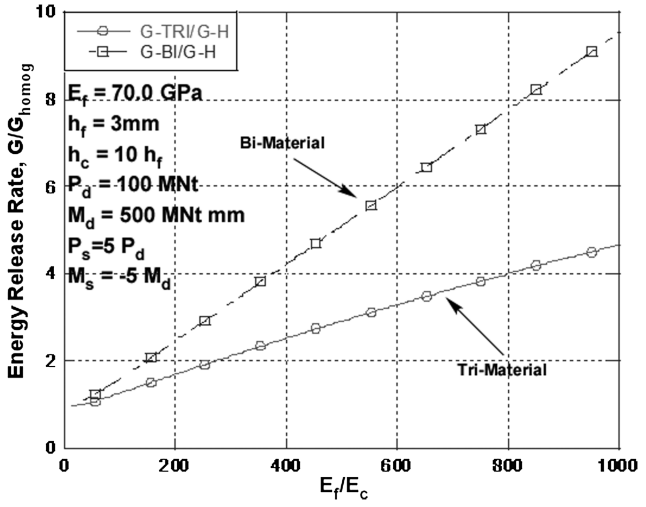

Fig. 6 Effect of face modulus on the energy-release rate.

To examine the influence of core modulus on the energy-release rate of a sandwich, we use the same loading as before, the same face sheet modulus $E_f = 70$ GPa and face sheet thickness $h_f = 3$ mm, and a core thickness $h_c = 10h_f$. We vary the core material, so that the ratio E_c/E_f can be as high as 1000. The results in Fig. 6 again show lower energy-release rate for the trimaterial case than the corresponding bimaterial case, with the gap between the tri- and the bimaterial formulas being larger for the more compliant cores (i.e., for a higher ratio E_c/E_f). In fact, for $E_c/E_f = 1000$, the energy-release rate from the trimaterial formula is about 50% less than that for the bimaterial case and about five times that of the homogeneous case.

VI. Conclusions

The J-integral was used to obtain a closed-form algebraic expression for the energy-release rate G for a debonded sandwich beam. The mode mixity was determined by deriving a closed-form expression in terms of the geometry, material, and applied loading and in terms of a single scalar quantity ω, which is independent of loading. This loading-independence of ω is proven by extensive numerical studies on sandwich configurations with either "soft" or "moderate" core. Thus, for a particular geometry and material, ω can be extracted from a single numerical solution for one loading combination. In the present analysis, the most general case of an asymmetric sandwich is considered (i.e., the bottom face sheet may not necessarily be of the same material and thickness as the top face sheet). These formulas extend the existing formulas in the literature, which are limited to a delamination in a homogeneous composite or an interface crack in a bimaterial beam.

Appendix A: Homogeneous Limit for the Energy-Release Rate

For the case of a homogeneous section, the debond is just a delamination at a distance h_{f1} from the top surface. Denoting the total thickness by t, the expression derived herein converges to the expression given by Yin and Wang [4]. In this case, denoting $\bar{h} = h_{f1}/t$, Eqs. (7b, 9b) become

$$C_1 = \bar{h}; \qquad C_2 = \frac{6\bar{h}(1-\bar{h})}{t}; \qquad C_3 = \bar{h}^3 \tag{A1}$$

and the energy-release rate for the homogeneous limit becomes

$$G = \frac{(1-\nu_{zx}\nu_{xz})}{2E_1 t^3}\left[\frac{(tP^*)^2}{\bar{h}(1-\bar{h})} + \frac{12M_d^{*2}}{\bar{h}^3} + \frac{12(tP^*/2 - M_d^*)^2}{(1-\bar{h})^3}\right] \tag{A2}$$

Appendix B: Bimaterial Limit for the Energy-Release Rate

The limit of a bimaterial is obtained from the present expression if we set $h_{f2} = 0$ (i.e., we only have the top face and the core). In this case, the present expression converges to the expression given by Suo and Hutchinson [5].

In terms of

$$\eta = \frac{h_{f1}}{h_c}; \qquad \Sigma = \frac{\bar{E}_{f1}}{\bar{E}_c} \tag{B1a}$$

where

$$\bar{E} = \frac{E}{1-\nu_{zx}\nu_{xz}} \tag{B1b}$$

and

$$\Delta = \frac{1 + 2\eta\Sigma + \eta^2\Sigma}{2\eta(1+\eta\Sigma)}; \qquad \beta = \Delta - \frac{1}{\eta}; \qquad A_0 = \frac{1}{\eta} + \Sigma \tag{B1c}$$

$$I_0 = \frac{1}{3}\left[\Sigma(3\beta^2 - 3\beta + 1) + 3\frac{\Delta}{\eta}\beta + \frac{1}{\eta^3}\right] \tag{B1d}$$

the constants in Eqs. (4c) and (5c) become

$$C_1 = \frac{\Sigma}{A_0}; \qquad C_2 = \frac{\Sigma}{h_{f1} I_0}\left(\frac{1}{2} - \beta\right); \qquad C_3 = \frac{\Sigma}{12 I_0} \tag{B2}$$

By also denoting

$$A = \frac{1}{1 + \Sigma(4\eta + 6\eta^2 + 3\eta^3)}; \qquad I = \frac{1}{12(1 + \Sigma\eta^3)}; \qquad \sin\gamma = 6\Sigma\eta^2(1+\eta)\sqrt{AI} \tag{B3}$$

the energy-release rate for the bimaterial limit becomes

$$G = \frac{(1 - \nu_{zx}^{(f1)}\nu_{xz}^{(f1)})}{2E_{f1}}\left[\frac{P^{*2}}{Ah_{f1}} + \frac{M_d^{*2}}{Ih_{f1}^3} - 2\frac{P^* M_d^*}{h_{f1}^2\sqrt{AI}}\sin\gamma\right] \tag{B4}$$

with P^* and M_d^* defined by Eqs. (7b, 9b) with C_i from Eq. (B2).

Acknowledgments

The financial support of the U.S. Office of Naval Research, grant N00014-07-10373, and the interest and encouragement of the Grant Monitor, Y.D.S. Rajapakse, are both gratefully acknowledged. Likewise, the financial support of the Danish Council for Independent Research, Technology and Production Sciences, grant 10–082020, partially making this work and a guest professorship at the Technical University of Denmark for Leif A. Carlsson possible, is gratefully acknowledged.

References

[1] Kardomateas, G. A., and Huang, H., "The Initial Postbuckling Behavior of Face-Sheet Delaminations in Sandwich Composites," *Journal of Applied Mechanics*, Vol. 70, No. 2, 2003, pp. 191–199. doi:10.1115/1.1532320

[2] Kardomateas, G. A., and Schmueser, D. W., "Buckling and Postbuckling of Delaminated Composites Under Compressive Loads Including Transverse Shear Effects," *AIAA Journal*, Vol. 26, No. 3, 1988, pp. 337–343. doi:10.2514/3.9894

[3] Kardomateas, G. A., "Large Deformation Effects in the Postbuckling Behavior of Composites with Thin Film Delaminations," *AIAA Journal*, Vol. 27, No. 5, 1989, pp. 624–631. doi:10.2514/3.10153

[4] Yin, W.-L., and Wang, J. T. S., "The Energy-Release Rate in the Growth of a One-Dimensional Delamination," *Journal of Applied Mechanics*, Vol. 51, No. 4, 1984, pp. 939–941. doi:10.1115/1.3167752

[5] Suo, Z., and Hutchinson, J. W., "Interface Crack Between Two Elastic Layers," *International Journal of Fracture*, Vol. 43, No. 1, 1990, pp. 1–18. doi:10.1007/BF00018123

[6] Ostergaard, R. C., and Sorensen, B. F., "Interface Crack in Sandwich Specimen," *International Journal of Fracture*, Vol. 143, No. 4, 2007, pp. 301–316. doi:10.1007/s10704-007-9059-4

[7] Budiansky, B., and Rice, J. R., "Conservation Laws and Energy-Release Rates," *Journal of Applied Mechanics*, Vol. 40, No. 1, 1973, pp. 201–203.

[8] Rice, J. R., "Elastic Fracture Mechanics Concepts for Interfacial Cracks," *Journal of Applied Mechanics*, Vol. 55, No. 1, 1988, pp. 98–103. doi:10.1115/1.3173668

[9] Hutchinson, J. W., Mear, M. E., and Rice, J. R., "Crack Paralleling an Interface Between Dissimilar Materials," *Journal of Applied Mechanics*, Vol. 54, No. 4, 1987, pp. 828–832. doi:10.1115/1.3173124

[10] Thouless, M. D., Evans, A. G., Ashby, M. F., and Hutchinson, J. W., "Edge Cracking and Spalling of Brittle Plates," *Acta Metallurgica*, Vol. 35, No. 6, 1987, pp. 1333–1341. doi:10.1016/0001-6160(87)90015-0

[11] Charalambides, P. G., Lund, J., Evans, A. G., and McMeeking, R. M., "A Test Specimen for Determining the Fracture Resistance of Biomaterial Interfaces," *Journal of Applied Mechanics*, Vol. 56, No. 1, 1989, pp. 77–82. doi:10.1115/1.3176069

[12] Sorensen, B. F., Jorgensen, K., Jacobsen, T. K., and Ostergaard, R. C., "DCB-Specimen Loaded with Uneven Bending Moments," *International Journal of Fracture*, Vol. 141, No. 1, 2006, pp. 163–176. doi:10.1007/s10704-006-0071-x

[13] Lundsgaard-Larsen, C., Sorensen, B. F., Berggreen, C., and Ostergaard, R. C., "A Modified DCB Sandwich Specimen for Measuring Mixed Mode Cohesive Laws," *Engineering Fracture Mechanics*, Vol. 75, No. 8, 2008, pp. 2514–2530. doi:10.1016/j.engfracmech.2007.07.020

[14] Carlsson, L. A., and Kardomateas, G. A., *Structural and Failure Mechanics of Sandwich Composites*, Springer, Dordrecht, The Netherlands, 2011, pp. 322–324.

[15] Berggreen, C., Simonsen, B. C., and Borum, K. K., "Experimental and Numerical Study of Interface Crack Propagation in Foam Cored Sandwich Beams," *Journal of Composite Materials*, Vol. 41, No. 4, 2007, pp. 493–520. doi:10.1177/0021998306065285

S. Pellegrino
Associate Editor